NURETH14-323

Laminar flame properties and Flame acceleration prediction of hydrogen-methane mixtures K. Coudoro^{1,2}, N. Chaumeix¹, A. Bentaib², and C.-E. Paillard¹

¹ Institut de Combustion, Aérothermique, Réactivité et Environnement CNRS Orléans, France

Abstract

The combustion of a binary mixture of methane and hydrogen has been studied using 2 different experimental setups: the spherical bomb to investigate the fundamental flame properties of this mixture with air, initially at 100 kPa, at different initial temperatures (300 - 363 K) and for a wide range of equivalence ratios (0.8 - 1.4); ENACCEF to investigate the flame acceleration phenomena in smooth tube for mixtures initially at ambient conditions and for equivalence ratios ranging between 0.57 and 0.84. A detailed kinetic mechanism has been used to derive the activation energies needed for the flame acceleration analysis.

Introduction

The occurrence of an accidental explosion as a result of flammable gases ignition that may be released in process industries is of a major concern. In most of the accidental situations, the ignition source is either an electrical spark or a hot surface, resulting in slow laminar flames which can accelerate under certain conditions and undergo transition to detonation generating overpressures high enough to cause severe material damages. Predicting and understanding the process of flame acceleration therefore became key subjects in preventing industrial hazards. Flame acceleration has been largely studied for a homogeneous hydrogen distribution in the available containment volume [1-3] and a criterion has been proposed in order to assess the propensity of the flame to acceleration. The aim of the present work is to verify if this criterion can apply to mixtures with different characteristics such as natural gas which can vary in composition and may contain a large amount of hydrogen. This natural gas, enriched in hydrogen, represents a good candidate to extrapolate the hydrogen criterion regarding flame acceleration. Concerning the fundamental properties, if both hydrogen/air and methane/air mixtures have been extensively studied, only scarce data can be found in the literature concerning hydrogen/methane/air mixtures. The aim of the present work is to determine the fundamental properties of a hydrogen/methane/air mixture since it constitutes one of the reference mixture to assess flash-back hazards on burners using natural gas: 77% molCH4, 23% molH2 (G222) and predict the acceleration potential of these flames. Laminar flame velocities and Markstein lengths were determined experimentally by studying expanding spherical flames in a combustion bomb using high speed imaging coupled to a schlieren optical setup. The experimental laminar flames speed data were used in order to validate a detailed kinetic mechanism for G222/air combustion based on published mechanisms using COSILAB-1D freely propagating flame. Transport properties as well as the flame temperature, the maximum theoretical pressure and the expansion ratio were estimated using CHEMKIN II equilibrium calculations. Using the chosen detailed chemical kinetic mechanism aforementioned, the activation energies were derived from the D:\Serge\SERGE\Communications\Nureth\NURETH-14-VP.doc

² Institut de Radioprotection et de Sureté Nucléaire, DSR/SAGR, Fontenay-aux-Roses, France

evolution of laminar flame velocities as a function of the flame temperature (COSILAB-1D freely propagating flame). The effect of the initial temperature (from 300 K up to 370 K) on the different properties was examined.

Propensity to acceleration of lean mixtures was then studied in a highly instrumented 5 meters long vertical facility: ENACCEF. The facility displays a dome: a 685L vessel connected to a 3.3 meters long acceleration tube that can be equipped with obstacles. The initial temperature and pressure were at ambient condition. The experiments were conducted in smooth conditions.

1. Laminar flame study

1.1 Experimental setup and methodology

1.1.1 <u>Experimental setup</u>

The experimental setup used in this work is composed of a stainless steel spherical combustion chamber (476 mm inner diameter and 561). The chamber is equipped with 4 quartz windows (97 mm diameter) in order to provide an optical access during flame propagation (fig1-(a). The ignition is obtained via the production of an electrical spark generated by a high voltage source between 2 electrodes (fig1-(b)).

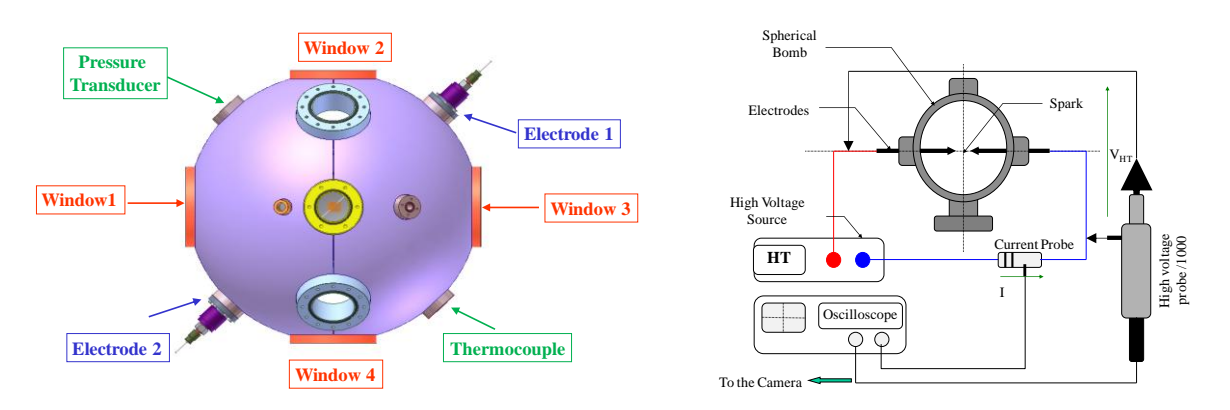


Figure 1:Experimental setup. (a)- Schematic of the spherical vessel; (b) Ignition system.

When a mixture is flammable, providing an ignition source will lead to the onset of a combustion wave that will spread inside the vessel until all the fresh gases have burnt. The initial flame kernel created by the spark will increase in size outwardly. Using a Schlieren technique, the flame front can be visualized as it propagates in the vessel. An example is given in Figure 2 with a series of images captured by the high speed camera in the case of a stoichiometric mixture of G222/ air initially at 100 kPa and ambient temperature. One can see that a smooth flame expands in the vessel with a well defined flame front. The high speed camera records the images of the flame propagation allowing the evaluation of the flame radius as a function of time using a in-house program based on Matlab tools. Since previous studies [1, 2], the tracking technique has been improved in order to have a better estimate of the flame radius from the schlieren images. On each image, the localization of the flame front is detected and each corresponding pixel coordinates are stored. A flame radius according to the angle can be then determined and an average is calculated.

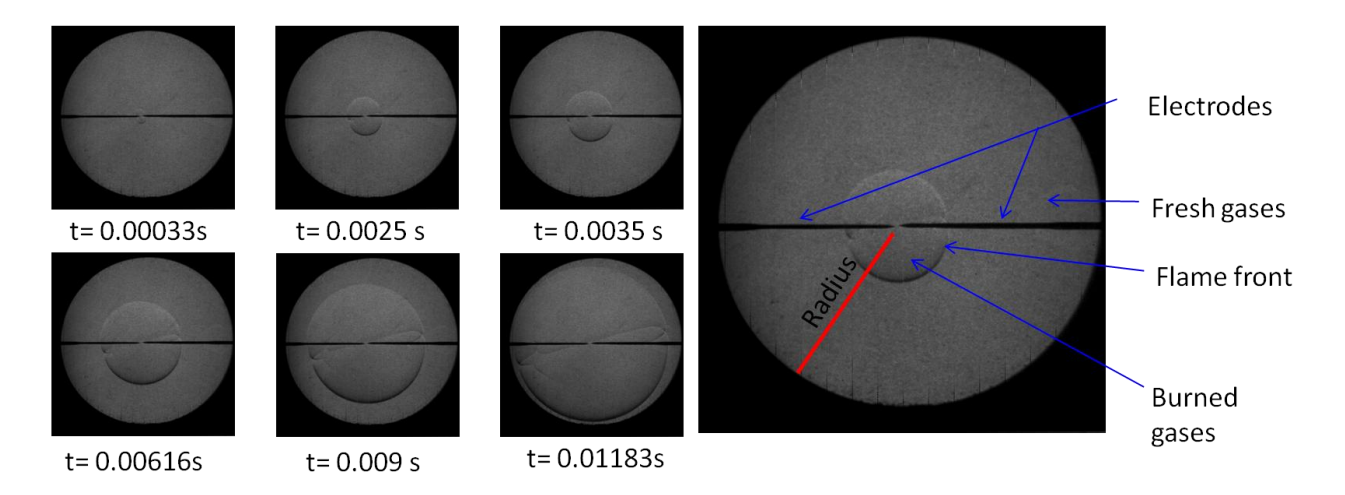


Figure 2: Temporal evolution of the flame front (equivalence ratio=1.05, P=1 bar, T=363K)

Before each test, the chamber was vacuumed and the residual pressure was lower than 3 Pa. The gases were introduced directly in the vessel using the partial pressure method. The laboratory dry air consisted of $0.21 O_2 + 0.79 N_2$. The fuel mixture was constituted of $77\%_{mol}$ CH₄ and $23\%_{mol}$ H₂ it was supplied by Air Liquide with a purity better than 0.9999. The partial pressure was measured using capacitive manometers (MKS) of different full scales according to the desired pressure (10^2 Torrs) and 10^3 Torrs . Based on the precision of the capacitive manometers, the mixtures were obtained with an accuracy of 0.2%.

1.1.2 Methodology

The methodology used to derive the laminar flame velocity from expending spherical flames was largely exposed by Lamoureux et al. [4] and Halter et al.[5] and will be here briefly described. As it has been mentioned earlier, the flame radius for each image can be derived and consequently the evolution of the radius versus time as it is shown in fig. 3.

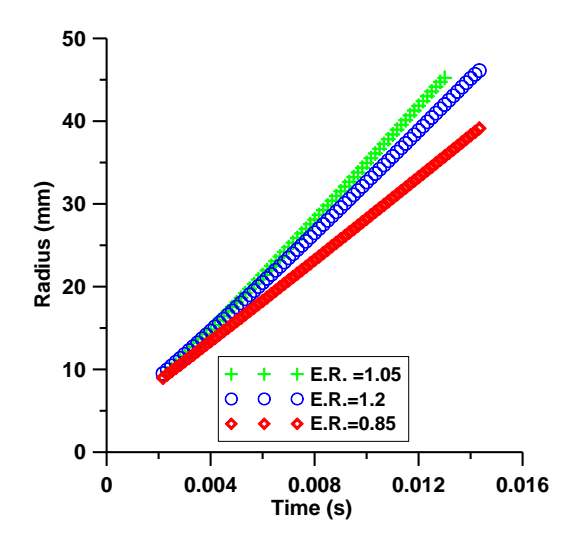


Figure 3: Temporal evolution of the flame front radius for three different equivalent ratios (P=1 bar, T=333K)

The flame is assumed to be spherical with a smooth surface such as the flame surface corresponds, at each time, to the envelop of the sphere. In this case, the spatial velocity reflecting the flame propagation speed is derived from the flame radius versus time data:

$$V_{S} = \frac{dr_{b}}{dt} \tag{1}$$

where r_b is the radius of the flame and t is the time. Eschenbach and Agnew [6] proposed the following expression to derive the laminar flame velocity as function of the spatial velocity:

$$S_{L} = \left(V_{S} + \frac{r_{b}}{3P_{b}} \cdot \frac{dP_{b}}{dt}\right) \cdot \left(\frac{M_{b} \cdot T_{u} \cdot P_{b}}{M_{u} \cdot T_{b} \cdot P_{u}}\right)$$
(2)

with M being the molar mass; P, T, the pressure and temperature; u the relative to unburnt gas and b the relative to burnt gas; r_b the flame radius and t the time. At the early stages of the combustion, when the radius of the flame is smaller than the radius of the enclosed volume, the burnt gases volume is too low to induce any pressure increase, which can be considered as equal to the initial one. The pressure being constant, the expression of the laminar flame speed becomes:

$$S_{L} = (V_{S}) \cdot \left(\frac{M_{b} \cdot T_{u} \cdot P_{b}}{M_{u} \cdot T_{b} \cdot P_{u}} \right)$$
 (3)

With $\sigma = \frac{M_u \cdot T_b \cdot P_u}{M_b \cdot T_u \cdot P_b} = \frac{\rho_u}{\rho_b}$ being the expansion factor of the burnt gases

However the spherically propagating flame is submitted to curvature and strain effects that imply a modification in the flame surface. The relative change in the flame surface is the flame stretch and in the case of a spherically expanding flame the stretch rate is:

$$\kappa = \frac{1}{A} \cdot \frac{dA}{dt} = \frac{2 \cdot V_S}{r_b} \tag{4}$$

Therefore, the effect of stretch needs to be taken into account when we evaluate the laminar flame velocity: V_S being the stretched spatial velocity and V_S° the unstretched spatial velocity. Both velocities are linked by a coefficient known as the Markstein length L. The following relation was proposed by Clavin (1985) [7].

$$V_S = V_S^0 - L \cdot \kappa \tag{5}$$

The fundamental flame velocity is also submitted to stretch effects:

$$S_L = S_L^0 - L' \cdot \kappa \tag{6}$$

Where L' represents the Markstein length divided by the expansion factor and S_L^0 the unstretched fundamental flame velocity.

1.2 Experimental results and modelling the activation energy

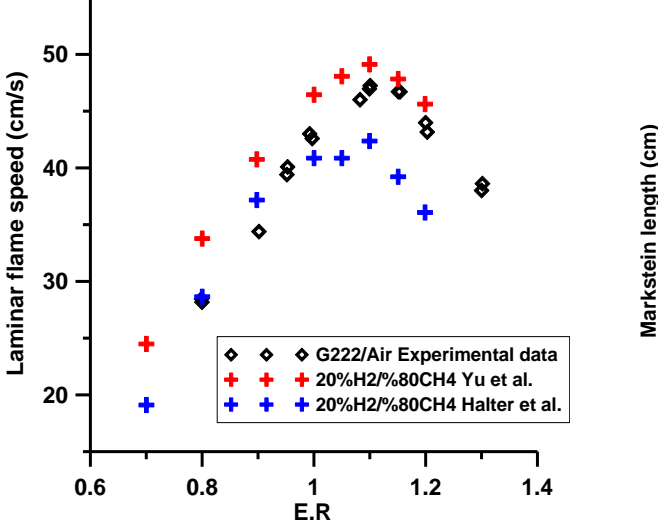
1.2.1 G222/Air flames at 1 bar and 303K

Laminar flame speed and Markstein length

The unstretched laminar flame velocity has been determined for an equivalence ratio (E.R) between 0.7 and 1.4 at 3 different initial temperatures, 303, 333 and 363 K for a total pressure of 100 kPa. As it has been reported in section1.1.2, the visualization of the flame is possible up to a flame diameter of 97 mm. Hence, when the flame reaches the maximum radius that can be visualized, the volume of the burnt gases is approximately 0.8 % of the total volume of the spherical bomb which cannot be responsible of any pressure increase as it will be shown in the following sub-section.

Figure 4 shows the evolution of the laminar flame velocity for G222/Air mixtures as a function of the equivalent ratio with the pressure set at 1 bar and ambient temperature. The plot exhibits a bell shaped evolution of the laminar flame velocity. The laminar flame velocity increases from the lean side up to a maximum value of 47.2 cm/s for an E.R of 1.1 and then decreases with the increase of the E.R

As there is no data on G222 in the literature, we compare our data to those on H_2 -CH₄ (20%-80%)/Air by Halter et al. [5] and Yu et al.[8]. The velocities proposed by Yu et al. seem too high when compared to those of Halter et al. and to ours. This was explained by Halter as due to the experimental configuration of their counter flow burner. Figure 4 also show that G222 measured velocities are slightly higher than those proposed by Halter. This was expected as G222 contains a higher hydrogen proportion.



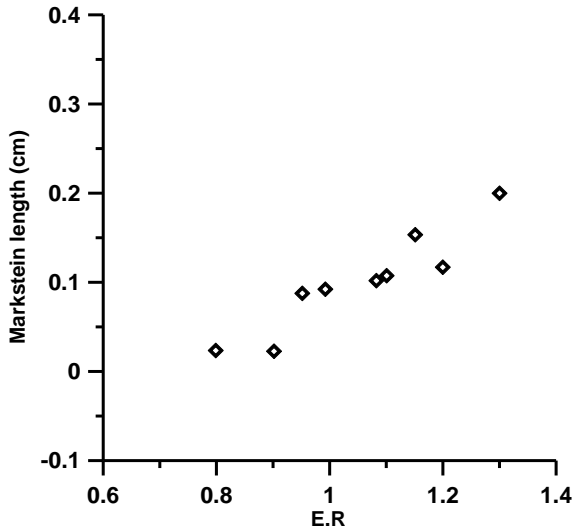


Figure 4: Laminar flame velocity for G222/air mixtures at 1bar and 303K as a function of the equivalence ratio (E.R.)

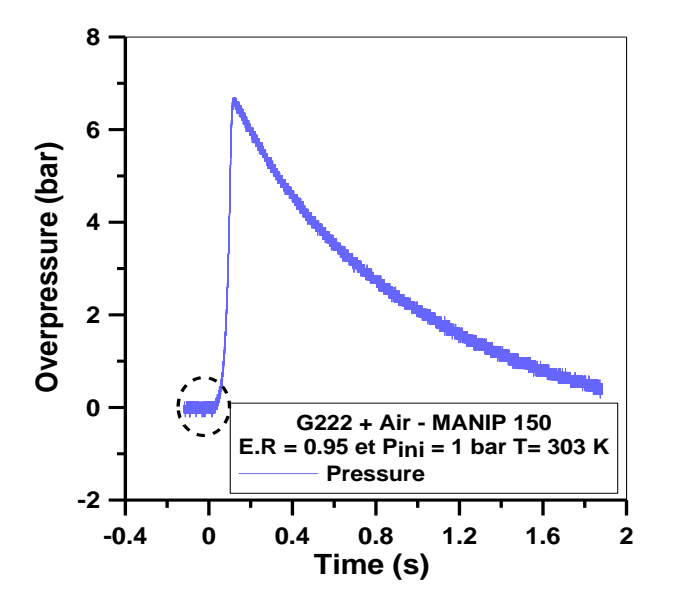
Figure 5: Markstein lengths for G222/air mixtures at 1bar and 303K as a function of the equivalence ratio (E.R.)

Figure 5 shows the Markstein length plotted against the equivalence ratio. The increasing equivalence ratio results in increasing the Markstein length. Also the Markstein length remains

positive sign of the flame stability. It is to be noticed that, as mentioned by Lamoureux et al.[4], Markstein lengths determination can be submitted to important errors.

Maximum combustion pressure

During flame propagation, we were able to record the pressure rise in the combustion chamber using a Kistler pressure sensor mounted inside the chamber. Figure 6 and Figure 7 show the pressure rise in the chamber as a function of the time as well as the visualization window. By monitoring the pressure during the combustion, it is shown that the pressure remains constant during flame visualization justifying the use of the constant pressure assumption in the early stages of the flame propagation.



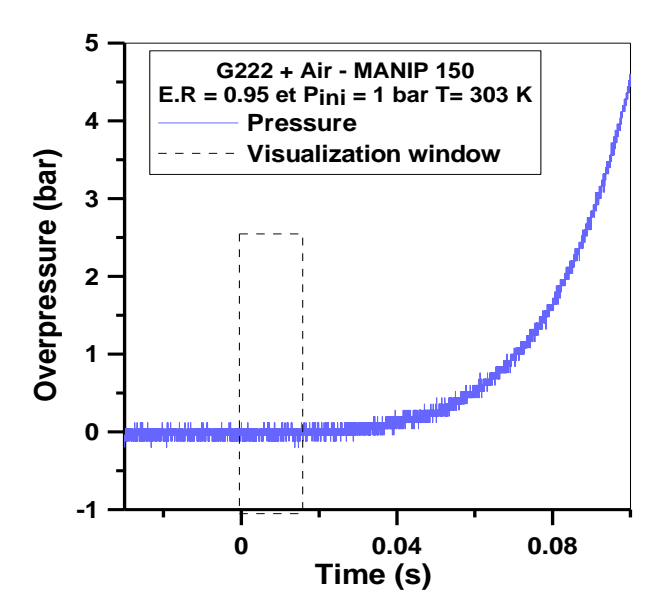
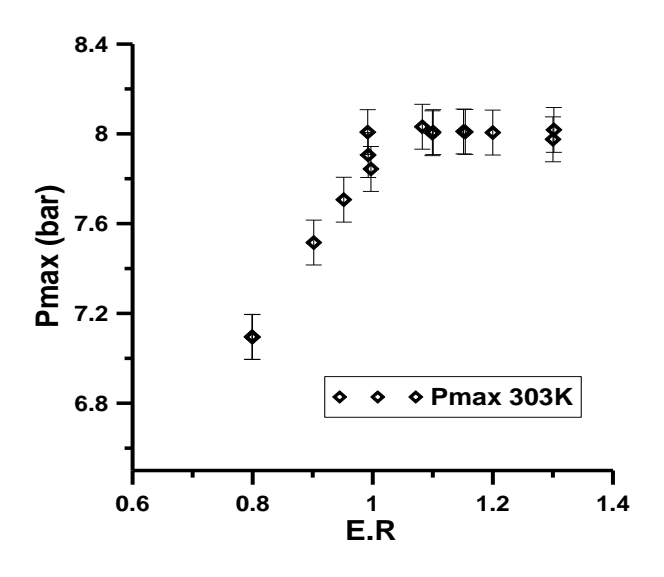


Figure 6: Pressure rise in the chamber for a G222/Air mixture with an equivalence ratio of 0.95, P=1bar and T=303K

Figure 7: Zoom on visualization window for a G222/Air mixture mixture with an equivalence ratio of 0.95, P=1bar and T=303K

The maximum combustion pressures were measured in the meantime (Figure 8) and compared to the theoretical adiabatic isochoric complete combustion pressures (PAICC) (Figure 9) estimated using CHEMKIN II equilibrium calculations. The error on the maximum pressure measurement is estimated to be around ± 0.1 bar.



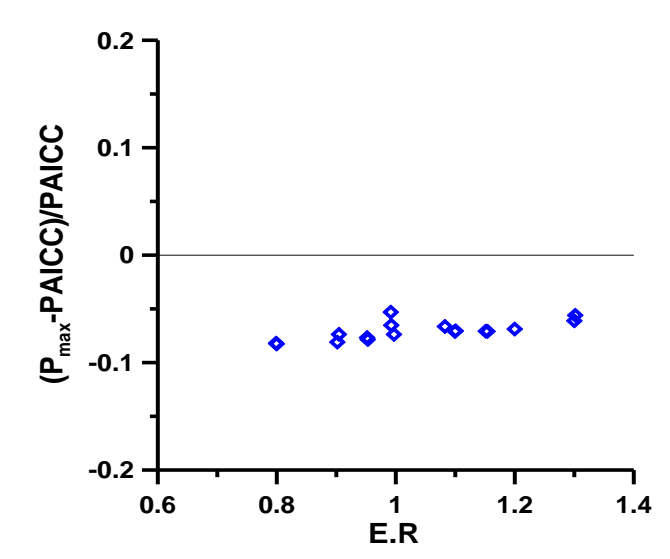


Figure 8: Measured maximum pressures as a function of the mixture equivalence ratio (E.R)

Figure 9: (P_{max}-PAICC)/PAICC versus the mixture equivalence ratio (E.R).

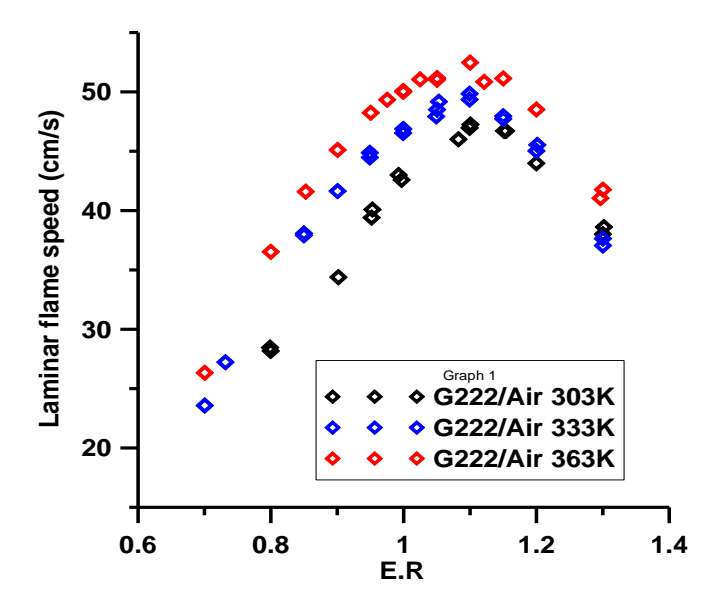
It appears on Figure 8 that the maximum pressures increase sharply from the lean side up to a maximum value of 8.0 ± 0.1 bar corresponding to an equivalence ratio. of 1.08. This increase is then followed by a slight decrease when going to the rich side of the mixture. When compared with the PAICC, as shown on Figure 9, we note that the measured maximum pressures are 10% lower than the PAICC. Such a difference is certainly due to the heat losses at the walls of the spherical bomb.

1.2.2 Effect of the initial temperature on the flame properties

Laminar flame speed and Markstein length

Figure 10 presents the effect of the initial temperature on the laminar flame velocity of G222/Air mixtures. Overall, we observe a global increase in the laminar flame velocity as the temperature increases. This results in a raise of the maximum velocity which augments from 47.2 cm/s at ambient temperature up to 49.6 cm/s when the temperature is set at 333K and then to 52.5 cm/s when the initial temperature is set at 363K. The equivalence ratio for which this maximum is observed remains the same: 1.1.

Figure 11 presents how the initial temperature affects the Markstein lengths. Though we observe a very slight raise with the increasing temperature, it doesn't seem significant enough to express clear trends if we take into account the large uncertainties in the Markstein length derivation mentioned by Lamoureux et al. [4].



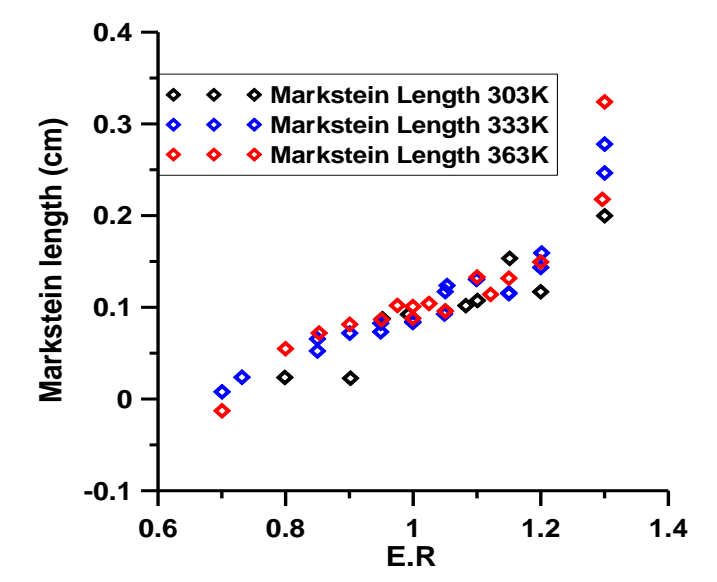


Figure 10: Effect of the temperature on the laminar flame velocity of G222/Air

Figure 11: Effect of the temperature on the Markstein lengths of G222/Air

Maximum combustion pressure

On figure 12 is shown the effect of the initial temperature on the measured maximum pressure. The curves present the same trend characterized by a fast increase from the lean side to the stoichiometry followed by an extremely slight decrease. Globally we observe a decrease of the overall curve as the initial temperature increases. With the initial temperature set at 303K, the highest value of the maximum pressure is 8.0 ± 0.1 bars. This value decreases to 7.4 ± 0.1 bars when the initial temperature is raised to 333K and decreases again to 6.9 ± 0.1 bars when the temperature is set to 363K.

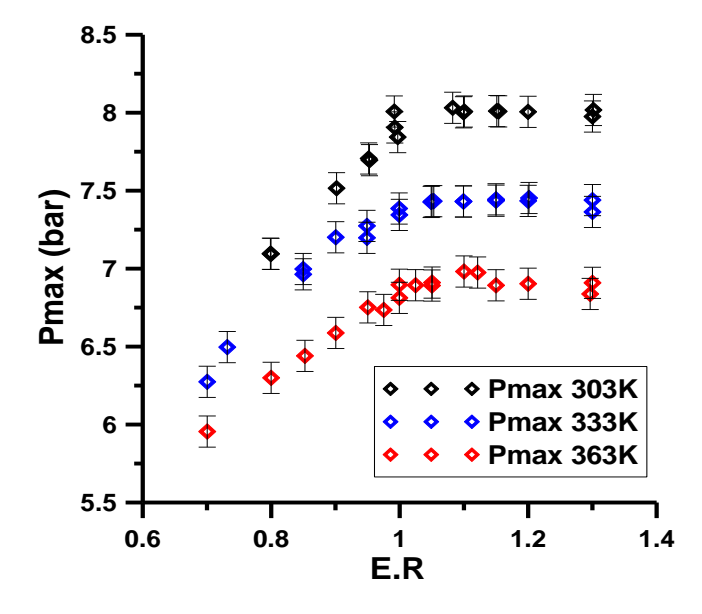


Figure 12: Effect of the temperature on the measured maximum pressures

1.2.3 Modelling the activation energy

The activation energies were computed using Cosilab-1D premixed flame alongside with the GRI3.0 detailed mechanism. The overall activation energy can be deduced from the simple Mallard – Le Chatelier approach who have shown that S_L must be in relation with the thermal diffusivity α and the reaction rate defined as a conversion rate ω . The analysis of Zeldovich for a reaction in a unique step following Arrhenius law shows that the laminar flame velocity is approximately linked with activation energy:

$$S_L^2 \approx A \cdot \exp\left(-\frac{E}{R \cdot T}\right)$$
 (7)

A being a coefficient, E the overall activation energy of the combustion reaction, and T_B the burnt gases temperature. Equation (7) finally permits to define the logarithm of the laminar flame speed as a function of the burnt gases temperature:

$$2 \cdot \ln(S_L) \approx \ln(A) - \frac{E}{R} * \frac{1}{T_R}$$
 (8)

The activation energies were evaluated by computing the laminar flame velocities for a fixed equivalence ratio by adding or subtracting 3% nitrogen using the chosen mechanism. This leads to a change in the flame laminar velocity and in the burnt gases temperatures while the equivalence ratio remains unchanged. The slope of the plot of the laminar flame speed as a function of the temperature *E*.

is
$$-\frac{E}{R}$$
.

Table 1 summarizes the results obtained using a detailed chemical kinetic mechanism [9] that was developed for natural gas combustion. The activation energy for an equivalence ratio of 0.8 was found equal to 167.6 kJ/mol. Two different behaviours are identified, on the lean side the activation energy increases up to 205.97 kJ/mol for the stoichiometric mixture. Then a drop is observed for an equivalence ratio of 1.1 for which the maximum flame speed is observed, then for higher equivalence ratios, the activation energy increases again with the equivalence ratio.

E. R.	Ea (kJ/mol)
0.8	167.6
0.9	182.43
1	205.97
1.1	53.95
1.2	174.12
1.3	220.03

Table 1: Activation energies for G222/air mixtures derived from detailed chemical kinetic calculations using 0D-laminar flame propagation.

2. Flame acceleration study

2.1 Experimental setup and initial conditions

The acceleration part of this study is being performed in a 5 long vertical facility: ENACCEF (Figure 13). The facility displays two distinct parts: (i) a 3.3 m long acceleration tube with an internal diameter of 0.154 m that can be equipped with obstacles; (ii)a 1.7 m long dome presenting an internal diameter of 0.538 m connected to the top of the acceleration tube

The acceleration tube can be obstructed with annular obstacles presenting different blockage ratios which represent the blocked surface of the tube by the obstacle. Here we present experiments made in smooth tube. 15 photomultipliers placed along the tube allow the flame detection and 7 pressure sensors mounted flush with the inner wall are used to measure the shockwave speed if applicable. Also, a Kistler sensor mounted behind a flame shield adaptor measures the evolution of the pressure during the combustion in order to derive the maximum pressure load. This sensor is located at the end of the acceleration tube.

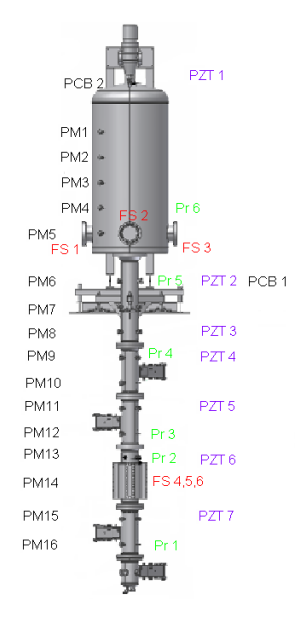


Figure 13: ENACCEF

In the following table, the initial conditions as well as the fundamental properties such as the expansion factor (σ) , the speed of sound in the burnt gases (Cs_{GB}) and the Lewis number for H_2 in the mixture are summarized. Each experiment has been repeated at least 3 times and was repeatable. The results are repeatable within $\pm 5\%$.

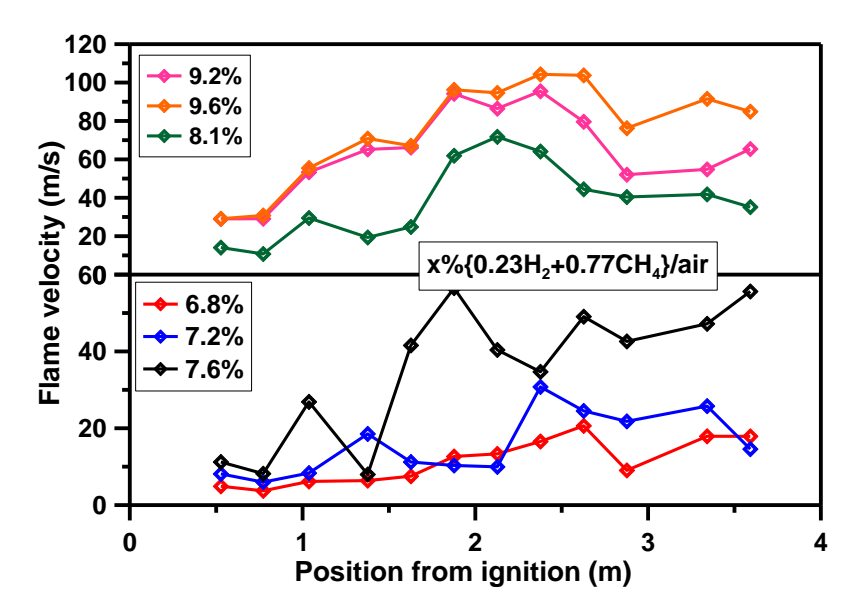
E.R	% _{G222}	σ	Cs _{GB} (m/s)	Le _{H2}
0.57	6.8	5.3553	864.75	0.29068
0.61	7.2	5.5686	880.85	0.29142
0.65	7.6	5.7778	896.22	0.29216
0.69	8.1	6.0332	914.43	0.29309
0.74	8.6	6.2813	931.49	0.294
0.80	9.2	6.5676	950.37	0.2951
0.84	9.6	6.7498	961.91	0.29584

Table 2: Experimental conditions

2.2 Flame propagation

The velocity of the flame is plotted against its position from the ignition point (Figure 14). For a given fuel content in the mixture, the flame velocity increases along the tube and generally reaches a maximum value at a distance between 2 and 3 m from the ignition point. The maximum value for a mixture containing $6.8 \%_{mol}$ G222 in air is about 20.5 m/s. Increasing the fuel concentration in the mixture leads to a strong increase of the maximum flame speed up to 102 m/s for a mixture

containing initially $9.6 \,\%_{mol}$ G222 in air. The level of velocity reached by the flame in the tube is greater than the one expected in the case of a laminar flame propagating in a tube. The profile of the velocity along the acceleration tube is similar for all the tested conditions. As its can be deduced from fig. 15, the overpressure inside the vessel increases as the flame propagates inside it. It reaches a maximum at the end of the combustion time, then it will decreases due to the heat losses to the wall leading to the cooling of the burned gases and hence to the condensation of the water vapour, leading to a pressure below the initial one (negative overpressure). The total combustion time is shortened in the dome part of ENACCEF. However, for all the studied conditions the maximum overpressure recorded by the pressure transducer remains below the theoretical one.



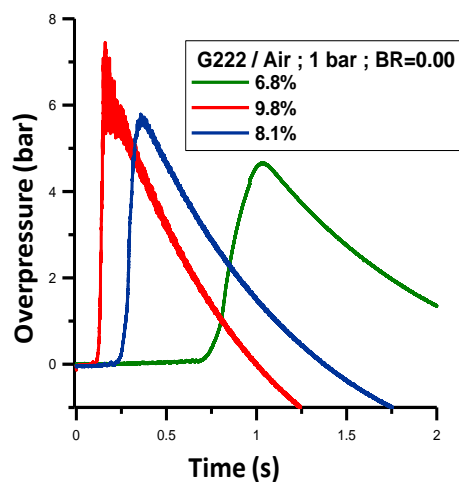


Figure 15; Pressure profile versus time in ENACCEF for 3 different percentage of fuel.

Figure 14: Flame velocity versus position from ignition

3. Conclusion

Laminar flame velocities and Markstein length have been evaluated for G222/air mixtures at 1 bar and temperature ranged between 303K and 363K. Moreover, we were able to measure the maximum combustion pressures which have been compared to the theoretical P_{AICC} . In future works $\left(\frac{dp}{dt}\right)_{max}$ will be also derived. Though activation energies were calculated in the process using the GRI3.0 mech, other mechanisms available in the literature will have to be tested and validated against the

experimental data in order to choose the one that give the best agreement with the experience. Also, the effect of flame acceleration on $\left(\frac{dp}{dt}\right)_{max}$ will be investigated. Finally, experiments in obstructed

tube will be conducted to derive an acceleration criterion for G222/air mixtures.

References

- 1. Yang, J.W., Z. Musiki, and S. Nimnual, *Hydrogen Combustion Control and Value-Impact Analysis for PWR Dry Containments*. 1991, NUREG/CR 5662.
- 2. Djebaïli-Chaumeix, N., et al., in *ICDERS Meeting*. 2003.
- 3. Dorofeev, S.B., et al. 1999, RRC Kurchatov Institute: Moscow.
- 4. Lamoureux, N., N. Djebaïli-Chaumeix, and C.E. Paillard, *Laminar flame velocity determination for H2-air-He-CO2 mixtures using the spherical bomb method*. Experimental Thermal and Fluid Science, 2003. **27**(4): p. 385-393.
- 5. Halter, F., et al., Characterization of the effects of pressure and hydrogen concentration on laminar burning velocities of methane-hydrogen-air mixtures. Proceedings of the Combustion Institute, 2005. **30**(1): p. 201-208.
- 6. Eschenbach, R.C. and J.T. Agnew, *Use of the constant-volume bomb technique for measuring burning velocity*. Combustion and Flame, 1958. **2**(3): p. 273-285.
- 7. Clavin, P., *Dynamic behavior of premixed flame fronts in laminar and turbulent flows*. Progress in Energy and Combustion Science, 1985. **11**(1): p. 1-59.
- 8. Yu, G., C.K. Law, and C.K. Wu, *Laminar flame speeds of hydrocarbon + air mixtures with hydrogen addition*. Combustion and Flame, 1986. **63**(3): p. 339-347.
- 9. Gregory P. Smith, D.M.G., Michael Frenklach, Nigel W. Moriarty, Boris Eiteneer, Mikhail Goldenberg, C. Thomas Bowman, Ronald K. Hanson, Soonho Song, William C. Gardiner, Jr., Vitali V. Lissianski, and Zhiwei Qin *GRI 3.0*. http://www.me.berkeley.edu/gri_mech/.